UNIVERSITY OF CALIFORNIA, MERCED

Assessment of Optical Performance of Three Non-Tracking, Non-Imaging, External Compound Parabolic Concentrators Designed for High Temperature Solar Thermal Collector Units

A thesis submitted in partial satisfaction of the requirements for the degree of
Master of Science in Environmental Systems

Presented by

Jesus Cisneros

May 1, 2010

THIS PAGE IS INENTIONALLY LEFT BLANK

The thesis of Jesus Cisneros is approved

_____

Jeff R. Wright

_____

Gerardo Diaz

_____

Roland Winston, Committee Chair

University of California, Merced

2010

THIS PAGE IS INENTIONALLY LEFT BLANK

Table of Contents

List of Figures

List of Tables & Charts

ABSTRACT OF THE THESIS

Assessment of Optical Performance of Three Non-Tracking, Non-Imaging, External Compound Parabolic Concentrators Designed for High Temperature Solar Thermal Collector Units

By

Jesus Cisneros

Master of Science in Environmental Systems

University of California, Merced, 2010

Professor Roland Winston, Chair

The objective of this thesis is to perform a preliminary optical assessment of the external compound parabolic concentrator (XCPC) component in three concentrating solar thermal units. Each solar thermal unit consists an optical element (the non-imaging concentrating reflector) and a thermal element (the evacuated glass tube solar absorber). The three concentrating solar thermal units discussed in this work are DEWAR 58, a direct flow all-glass dewar, DEWAR 47 an indirect flow all-glass dewar filled with thermal fluid and JIANG TUBE, a metal absorber with glass-to-metal seal. From the performance results, we will be able to determine the optical efficiency of the XCPC reflectors as well as the concentration ratio for radiation being transferred from the sun onto each of the three solar thermal collectors.

Assessment of Optical Performance of Three Non-Tracking, Non-Imaging, External Compound Parabolic Concentrators Designed for High Temperature Solar Thermal Collector Units

1 Introduction

Increased production costs in petroleum as well as negative environmental effects as a consequence of burning fossil fuels have prompted a search for low-cost, environmentally friendly technologies as an alternative. Solar thermal energy has the potential to replace petroleum and other fossil fuels as a high temperature heat source in many commercial and industrial technologies. However, production of a significant energy source of solar thermal heat for commercial and industrial use requires temperatures to reach well above the boiling temperature of water. For example, current commercially available double effect absorption cycle chillers require firing temperatures in the range of 150°C to 200°C. Flat-plate and simple evacuated tubes that reach temperatures of about 95°C are adequate for producing heat for residential hot water systems; however, alone cannot reach temperatures needed for commercial use.

At the University of California, Merced's Energy Research Institute (UC MERI), researchers are currently developing a solar-thermal energy system that is modular, low-profile, scalable and able to increase the temperature of a heat transfer fluid to output temperatures above 200°C. By achieving these temperatures, the solar energy can serve as a renewable energy source in applied technologies such as refrigeration, air conditioning, power generation, as well as water treatment and desalination systems.

This thesis is part of the ongoing UC MERI "High Temperature Solar-Thermal Collector" applied research project. The objective of this thesis is to perform a preliminary optical assessment of the external compound parabolic concentrator (XCPC) component in three concentrating solar thermal units. Each solar thermal unit consists an optical element (the non-imaging concentrating reflector) and a thermal element (the evacuated glass tube solar absorber). The three concentrating solar thermal units discussed in this work are:

1. DEWAR 58: direct flow all-glass dewar
2. DEWAR 47: indirect flow all-glass dewar filled with thermal fluid
3. JIANG TUBE: metal absorber with glass-to-metal seal

This paper focuses on the optical efficiency of the system and will show that using an external compound parabolic concentrator (XCPC), the optical component is able to operate with an optical efficiency above 60%. By achieving this goal, the total solar thermal unit has the potential to reach the larger project goal of an overall total system solar thermal efficiency of 50% operating at a temperature of 200°C. Section two of this thesis presents background information regarding solar concentration and ideal solar reflector design. Sections three and four present a detailed overview of the material and collector properties, physical dimensions as well as the XCPC properties and specifications. In section five, the results from the optical assessment are provided. Lastly, a discussion of the optical performance assessment is provided in section six, in fact showing that each of the XCPC reflectors has the potential to reflect enough radiation needed to warm the solar absorber to temperatures above 200°C.

2 Understanding Solar Concentration

To reach high system efficiencies in the solar thermal units with non-tracking solar collectors at temperatures above 200°C, it is not enough to eliminate convective and conductive losses by vacuum and reduce radiative losses by using a spectrally selective coating on the absorber (Welford and Winston, 1989). The purpose of the external compound parabolic concentrator (XCPC) is to increase the power density of solar radiation on the evacuated tubes. Although the concept of non-imaging concentrators has been around for about 30 years, price in glass manufacturing of solar absorber tubes has drastically gone down and warrants a re-examination of the potential to couple non-imaging concentrators with solar thermal applications.

2.1 Non-Imaging Optics

The field of non-imaging optics was first discovered by Roland Winston in 1969. The main difference between image-forming optical systems and non-imaging optical systems is that imaging optics must preserve the same spatial distribution of the incoming light where as non-imaging optics must only preserve the total space and energy but not the individual distribution. To better understand the differences, lets take a real life example. If we have a bowl of alphabet soup and spell out a word such as “SOLAR”, each letter will represent a light ray. Our goal is to transfer the rays or in this case letters from one point or plane to another. How will each of our imaging systems transfer the letters? In imaging systems, the letters that spell out the word “SOLAR” must remain in the same order as we transfer the location of the soup bowl. By contrast, in non-imaging optics, the

order of the letters is not important, however, conserving the total number of letters in the soup bowl as we transfer them from location A to location B is. Real life examples of imaging optics tools include cameras, telescopes, and microscopes. Figure 1.2 illustrates the fundamental difference expressed above, between an imaging and a nonimaging optical system.

2.2 The Theoretical Limit of Concentration

The concentration of sunlight via radiation is subject to fundamental limitations. Concentration of solar radiation is achieved by reflecting or refracting the flux incident on an aperture area A_a onto a smaller reflector or absorber area A_r. An optical concentration ratio, CR_0 is defined as the ratio between the solar flux on the receiver I_r, to the flux on the aperture, I_a or $CR_0 = I_r/I_a$. The geometrical concentration ratio is the same as the optical but is based on the areas and is defined as $CR=A_a/A_r$ (Goswami et al 2000).

In solar concentrating applications, the theoretical concentration limit as defined by Hottel's crossed-string method is $CR_{max,2D} = 1/\sin\theta_{max}$ where θ_{max} represents the acceptance half-angle of the concentrating component. The acceptance half-angle represents one-half of the angular zone within which radiation is accepted by the receiver or absorber of the concentrator. The concentration limit in three dimensions is represented by $CR_{max,3D} = 1/\sin^2\theta_{max}$. Due to the law of conservation of etendue, any concentrating system must tradeoff between concentration ratio and aperture area. As the concentration ratio increases, so does the rejection of radiation from an increasing

number of directions (Welford and Winston, 1989). For nontracking solar concentrators, it is very important to achieve increased concentration by rejecting irradiance from certain directions in order address total system thermal losses. In other words, an ideal trough type reflector /absorber combination accepts all radiation from normal incidence up to a certain threshold angle and rejects all radiation from the other directions with higher incidence angles (Spirkl et al., 1998a).

2.3 Ideal Solar Reflector Design

The ideal reflector shape for a perfectly black tubular absorber and no gap between absorber and reflector was first derived by Winston and Hinterberger in 1975. Later, Rabl, in 1976, prescribed a differential equation for these ideal reflector shapes, given an arbitrary acceptance angle. In an ideal reflector shape, we assume the following:

- Idealization of 100% reflecting surfaces meaning that all rays with a projected incidence angle less than the prescribed angle in the design are redirected onto the absorber
- No gap between the reflector and the outer glass tube
- No edge ray effects from the glass
- Cost and size of reflector material are not taken into account

As described in Winston 2005, the basic CPC equation is defined as:

$$(r\cos\theta_{max} + z\sin\theta_{max})^2 + 2a'(1 + \sin\theta_{max})^2 r - 2a'\cos\theta_{max}(2 + \sin\theta_{max})^2 z$$
$$- a'^2(1 + \sin\theta_{max})(3 + \sin\theta_{max}) = 0$$

where r is the radius of the reflector, $2a'$ is the diameter of the exit aperture, and θ_{max} is the maximum acceptance angle. This equation will yield a two-dimensional reflector. By revolving the curve along the z-axis, we can translate this two-dimensional reflector into three-dimensions, with $r^2 = x^2 + y^2$. A more compact parametric form can be found by making use of the polar equation of the parabola. In terms of this angle and the same coordinates (r,z), the meridian section is given by

$$r = ((2f\sin(\phi - \theta_{max})) / (1 - \cos\phi)) - a'$$

$$z = ((2f\cos(\phi - \theta_{max})) / (1 - \cos\phi)) - a'$$

where $f = a'(1 + \sin\theta_{max})$ and ϕ represents the angle of elevation. If we introduce an azimuthal angle Ψ we obtain the complete parametric equations of the XCPC surface:

$$x = ((2f\sin\Psi\sin(\phi - \theta_{max})) / (1 - \cos\phi)) - a'\sin\Psi$$

$$y = ((2f\cos\Psi\sin(\phi - \theta_{max})) / (1 - \cos\phi)) - a'\cos\Psi$$

$$z = ((2f\cos(\phi - \theta_{max})) / (1 - \cos\phi)) - a'$$

3 Design Specifications for Solar Thermal Collectors

Solar collector design specifications were already determined as this thesis is a small part of a larger applied research project. Performance assessment and design of the collectors were based on the specifications described in the sections below. An objective of this thesis is to assess the performance of each XCPC reflector in order to determine if the design is able to achieve an optical efficiency of at least 60 percent, and have a concentration ratio of at least 1.5. As an overall system, each unit design will have very similar optical components but differ in the method of heat transfer and its thermal components.

Several different approaches could have been taken to facilitate the vacuum-sealed solar collectors achieve the desired system efficiency and temperature. These include increasing the number of solar collectors to the system, adding a motorized sun-tracker to the collectors, designing a non-tracking internal compound parabolic concentrator into each solar collector and designing a non-tracking external compound parabolic concentrator (XCPC) for each solar collector. For the purposes of this thesis, the approach taken to reach the desired temperatures was designing a non-tracking XCPC with an optical performance of at least 60% and a concentration ratio of at least 1.5.

Each of the formulated designs consists of an assembly of stationary evacuated tube absorbers with external non-imaging reflectors to maximize concentration and optical efficiency on the collector.

The three design concepts that have been formulated are:

1. DEWAR 58: direct flow all-glass dewar
2. DEWAR 47: indirect flow all-glass dewar filled with thermal fluid
3. JIANG TUBE: metal absorber with glass-to-metal seal

3.1 Solar Thermal Unit Design #1 – DEWAR 58

The first of the solar thermal unit designs is DEWAR 58 - the direct flow all-glass dewar. The individual solar collector is depicted in figure 3.1 and the solar thermal design is depicted in figure 3.2. Table 3.1 shows a summary of materials and specifications used in the optical performance assessment.

In the DEWAR 58 solar thermal unit, the heat transport fluid flows directly inside the all-glass dewars, hence we use the term "direct flow." The design uses very inexpensive all-glass dewar solar thermal absorbers that are mass-produced in China. The dewars are cylindrical borosilicate glass bottles with an evacuated annulus between the two glass walls. The vacuum surface of the inner wall is coated with a selective surface (usually aluminum nitride cermet) with a high solar absorptance and low thermal emittance.

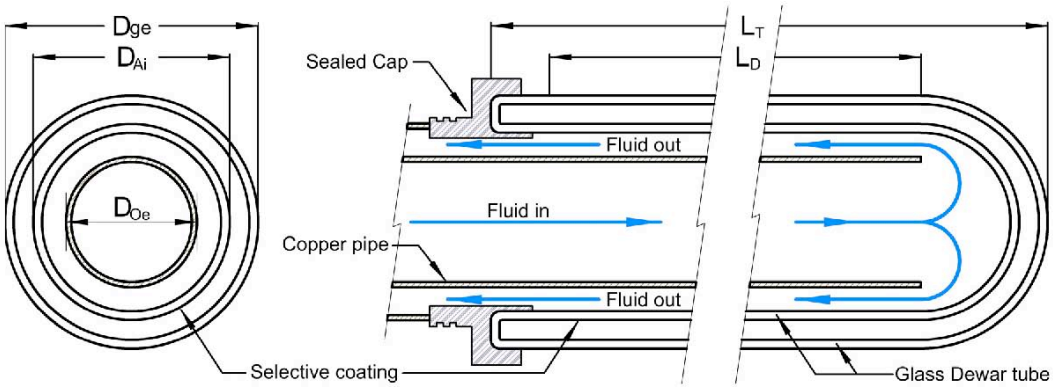

Figure 3.1. Cross sectional view of Dewar 58 Solar Collector Absorber

Fluid is fed into each dewar through a central feed-tube, made of copper, to the bottom of the glass dewar where the flow reverses and then passes back in the annulus between the copper feed-tube and the inner dewar of the inner glass cylinder.

The glass dewars are attached to a plumbing manifold using o-ring compression seals. The inlet tube is integral to the manifold itself, which speeds field installation and also eliminates a potential leak path at the connection of the inlet tube to the manifold. The manifold is configured so that the outlet of one collector can feed into the inlet of an adjacent collector. Each dewar is placed so that an external reflector concentrates the solar irradiance onto the inner dewar wall with the selective coating. The shape of the reflector has been designed so that the entire sunlight incident on the aperture plane of the collector, within a defined angular acceptance angle, is redirected onto the 47mm outer dewar absorber. Ray traces were performed over the design acceptance angle range of +34 degrees to -34 degrees.

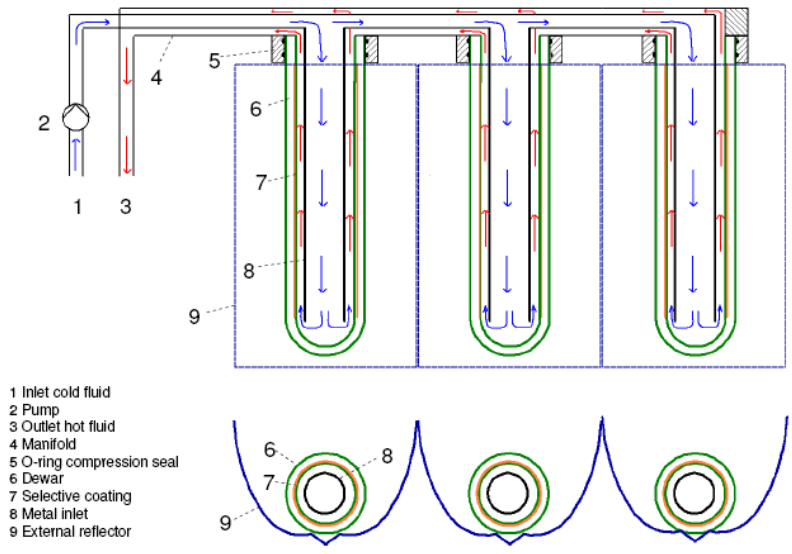

Figure 3.2. Cross sectional view of Dewar 58 Solar Thermal Collector Unit

The collectors will be oriented east-west; doing so will require smaller acceptance angles to ensure sufficient illumination throughout the day and avoid sacrificing concentration factor. Also, each dewar is placed so that an external reflector concentrates the solar irradiance onto the inner dewar wall with the selective coating.

Table 3.1. Design Specifications for Dewar 58 Solar Thermal Collector

COMPONENT	DESCRIPTION
Dewar Glass Type	Pyrex 7740
Internal Glass Dimensions	Inner Diameter = 43.8 mm Outer Diameter = 47.0 mm
External Glass Dimensions	Inner Diameter = 54.8 mm Outer Diameter = 58.0 mm
Vacuum Gas Pressure	$\leq 5 \times 10^{-3}$ Pa
Thermal Transfer Method	Direct fluid flow through copper pipe
Optical Properties of Glass	Refractive Index = 1.473 Transmittance = 91% Reflectance = 8% Absorbance = 1%
Selective Coating Type	Metal-Aluminum Nitride Cermet (Sputtering)
Selective Coating Dimension	Thickness = 0.1 mm – 0.3 mm
Optical Properties of Selective Coating	Absorptance = 94% Emittance = 5% Reflectance = 1%

3.2 Solar Thermal Unit Design #2 – DEWAR 47

The second of the solar thermal collector designs is DEWAR 47 - an indirect flow all glass dewar filled with thermal fluid. The individual collector design is depicted in figure

3.3 and the overall solar collector unit design is depicted in Figure 3.4. Table 3.2 shows a summary of materials and specifications used in the optical performance assessment.

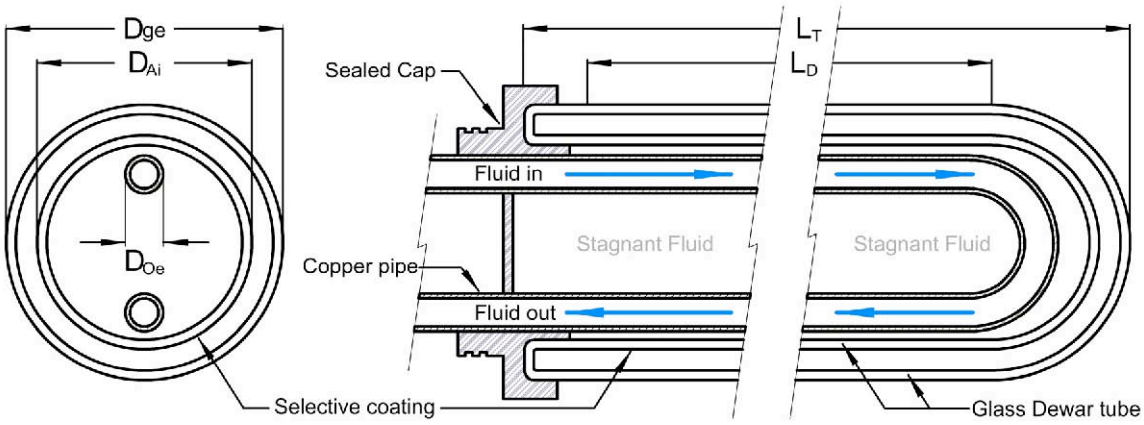

Figure 3.3. Cross sectional view of Dewar 47 Solar Collector Absorber

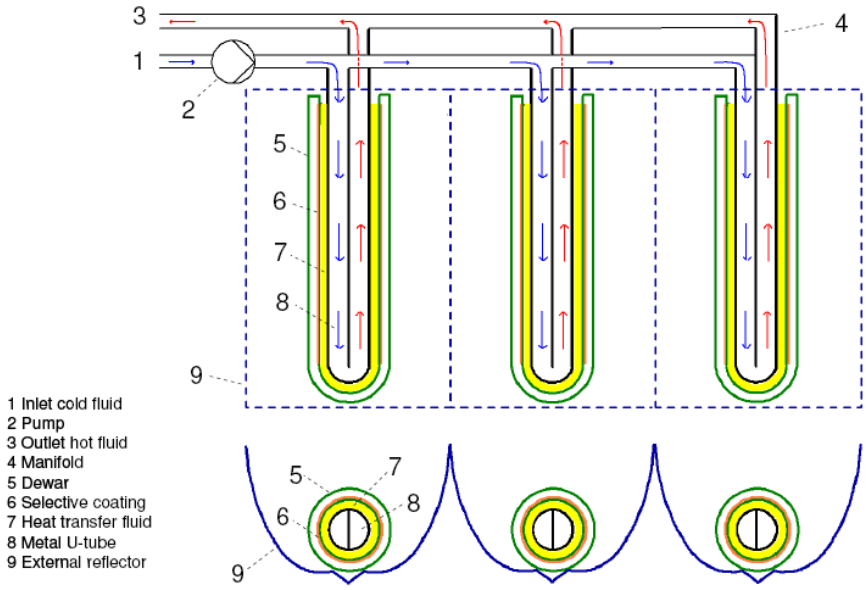

Figure 3.4. Cross sectional view of Dewar 47 Solar Thermal Collector Unit

The DEWAR 47 uses the same inexpensive all-glass dewar solar thermal absorber tubes as DEWAR 58, except in this concept design, the circulating fluid does not directly contact the glass dewars. The circulating fluid is confined to the manifold and the metallic tubes reaching into the glass dewars. Also, metallic inserts are immersed within a thermal fluid (e.g. a mineral oil) in order to enhance thermal transport from the blackened/coated inner dewar to the metallic insert.

Table 3.2. Design Specifications for Dewar 47 Solar Thermal Collector

COMPONENT	DESCRIPTION
Dewar Glass Type	Pyrex 7740
Internal Glass Dimensions	Inner Diameter = 33.8 mm Outer Diameter = 37.0 mm
External Glass Dimensions	Inner Diameter = 43.8 mm Outer Diameter = 47.0 mm
Vacuum Gas Pressure	$\leq 5 \times 10^{-3}$ Pa
Thermal Transfer Method	Indirect fluid flow through copper pipe
Optical Properties of Glass	Refractive Index = 1.473 Transmittance = 91% Reflectance = 8% Absorbance = 1%
Selective Coating Type	Metal-Aluminum Nitride Cermet (Sputtering)
Selective Coating Dimension	Thickness = 0.1 mm – 0.3 mm
Optical Properties of Selective Coating	Absorptance = 94% Emittance = 5% Reflectance = 1%

The other major difference between DEWAR 58 and DEWAR 47 is that the evacuated tubes must be oriented vertically (at a tilt) in order to contain the thermal fluid within the dewars. This requirement means that the XCPC must be designed to a larger acceptance angle (e.g. 60 degrees) because the sun traverses a wider range. The reflector shape and size is different for this design compared to that of design concept #1, but has been designed to yield the highest concentration ratio that is possible for a non-tracking solar collector with a +/- 60 degree acceptance angle.

3.3 Solar Thermal Design #3 – JIANG TUBE

The third of the solar thermal collector designs is the JIANG TUBE – a metal absorber with glass-to-metal seal. The solar collector absorber design is depicted in figure 3.5 and the total solar thermal unit design is illustrated in figure 3.6. Table 3.3 shows a summary of materials and specifications used in the assessment of optical performance.

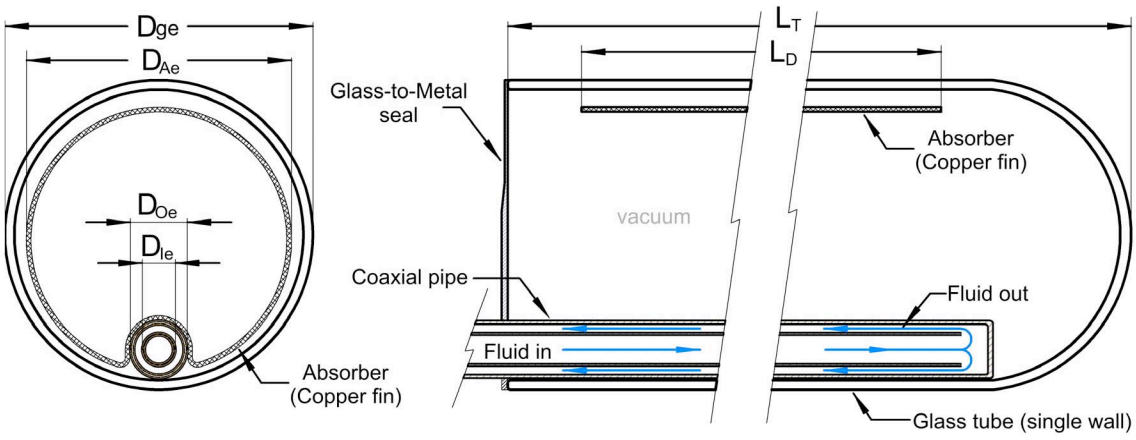

Figure 3.5. Cross sectional view of JIANG TUBE Solar Collector Absorber

The JIANG TUBE uses an evacuated glass tube with an innovative glass-to-metal seal at one end that maintains the vacuum to insulate the metal absorber. The metal absorber is a thin cylinder copper fin with a selective coating that enables high solar absorptance and reduces radiative heat loss. The fin is welded to a heat pipe, which transfers the heat absorbed to the manifold. As in the previous two concepts, the collectors will be oriented east-west. However, in Concept 3, each collector is placed so that an external reflector concentrates the solar irradiance onto the copper fin with the selective coating.

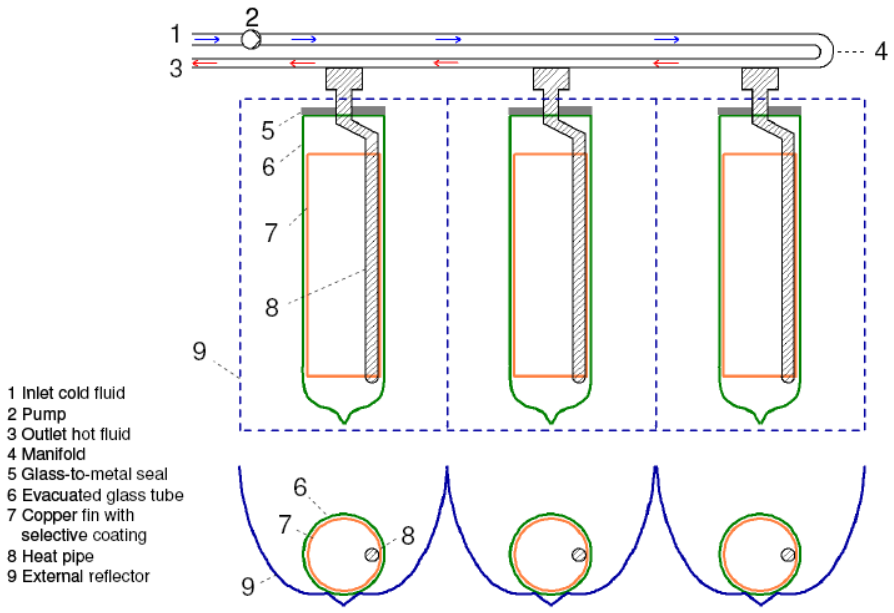

Figure 3.6. Cross sectional view of JIANG TUBE Solar Thermal Collector Unit

Table 3.3. Design Specifications for JIANG TUBE Solar Thermal Collector

COMPONENT	DESCRIPTION
Dewar Glass Type	Pyrex 7740
Internal Glass Dimensions	Inner Diameter = 52.8 mm Outer Diameter = 56.0 mm
External Glass Dimensions	Inner Diameter = 61.8 mm Outer Diameter = 65.0 mm
Vacuum Gas Pressure	$\leq 5 \times 10^{-3}$ Pa
Thermal Transfer Method	Copper fin absorber transfers heat to fluid in copper pipe
Optical Properties of Glass	Refractive Index = 1.473 Transmittance = 91% Reflectance = 8% Absorbance = 1%
Selective Coating Type	Metal-Aluminum Nitride Cermet (Sputtering)
Selective Coating Dimension	Thickness = 0.1 mm – 0.3 mm
Optical Properties of Selective Coating	Absorptance = 94% Emittance = 5% Reflectance = 1%

4 XCPC Reflector Design Specifications

The ideal reflector shape for a perfectly black tubular absorber and no gap between absorber and reflector was first derived by Winston and Hinterberger in 1975. Later, Rabl, in 1976, prescribed a differential equation for these ideal reflector shapes, given an arbitrary acceptance angle. In an ideal reflector shape, we assume the following:

- Idealization of 100% reflecting surfaces meaning that all rays with a projected incidence angle less than the prescribed angle in the design are redirected onto the absorber
- No gap between the reflector and the outer glass tube
- No edge ray effects from the glass
- Cost and size of reflector material are not taken into account

4.1 Overview of XCPC Reflector Design Process

Taking into account various real life factors, a customized XCPC reflector was designed for each of the solar collector conceptual models. The reflectors were designed to be as close as possible to an ideal reflector shape. A computer program was developed to illustrate the shape of the reflector curve and extract the necessary XCPC data sets needed to develop reflector shapes for each of the conceptual models. From the software, we are able to extract data points representing the shape of a two dimensional XCPC reflector curve. Next, the points are transferred to a three-dimensional computer-modeling program and the reflectors are digitally designed to real-life specifications for optical analysis and a ray trace. The detailed process is summarized next.

Step-by-Step Design Process for XCPC Reflectors

Step 1: Define the size of the absorber tubes. This includes the outer glass dimensions as well as the internal glass or copper absorber. In the case of this project, off-the-shelf commercially available products determined the size of the absorber tubes. Specifications can be found in section 3 of this thesis.

Step 2: Determine the desired reflector acceptance angle. For this project, analysis was performed to determine the optical efficiency for solar collectors oriented in north-south as well as east-west directions. Based on the geographic location where laboratory testing will be performed on the solar thermal system, it was concluded that for all conceptual designs, an acceptance angle of ±34° would be prescribed for east-west orientation and ±60° for north-south orientation.

Step 3: The virtual absorber. A technique used to reduce losses due to low absorptance at grazing incidence is the virtual absorber. In this case, rays that would miss the smaller virtual absorber design, still hit the larger actual absorber. However, one needs to take account that by taking this approach, there is a tradeoff between retaining the desired sharp cutoff angle and enhancing absorption by creating a cavity effect and avoiding grazing incidence. The virtual absorber technique was used in the computer model. Figure 4.1 shows a cross sectional view of the virtual absorber concept.

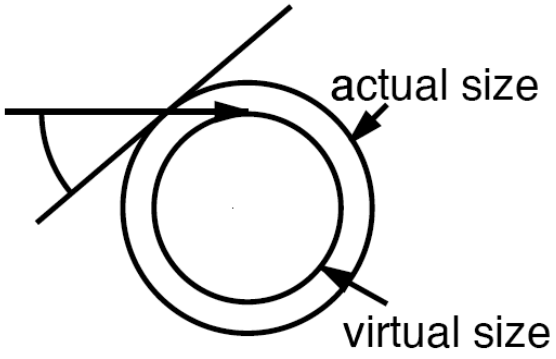

Figure 4.1. The Virtual Absorber

Step 4: V-grove technique to reduce gap losses. A technique used to reduce efficiency losses due to the gap between the XCPC reflector and the outside of the glass tube is the "V-groove technique". After an analysis was done, it was found that using this technique would only increase efficiency by less than 1%. While the V-groove effectively suppresses gap losses, it was determined that the losses were negligible when compared to the added complexity and cost of adding a V-groove to the reflector production and manufacturing.

Step 5: Input the desired collector specifications into the computer program. After all the design specifications were determined, Matlab version 3.5, was used to calculate the shape of the full reflector curve for an ideal XCPC using the set of parametric equations outlined in the previous sections. Figure 4.2 illustrates the cross sectional representation of the absorber and collector in Matlab.

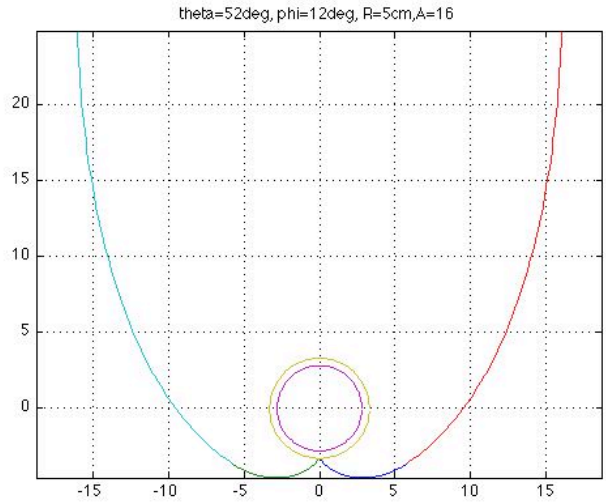

Figure 4.2. Cross sectional view of reflector and absorber using Matlab

Step 6: Export the data point set for each XCPC reflector half-curve. Each reflector curve data point set was exported to a spreadsheet for analysis. From this, we are able to verify the geometry of the curve as seen in Figure 4.3.

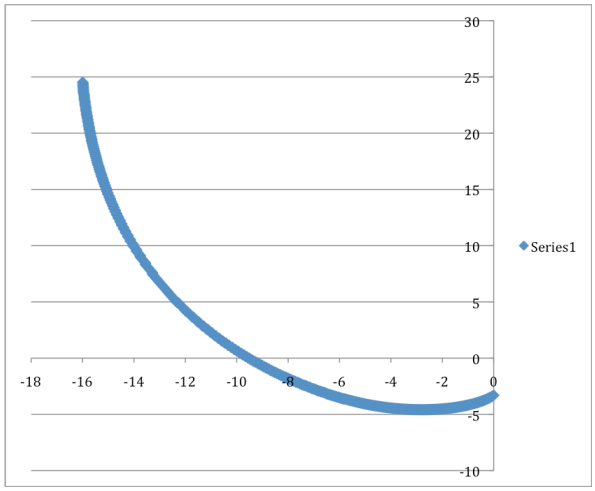

Figure 4.3. Geometric verification of reflector half-curve

Step 7: Reflector truncation. As mentioned before, the curve extracted from Matlab is for an ideal XCPC reflector. This gives optical conditions that are maximized for a desired acceptance angle and solar collector specifications. The ideal reflector will need to be truncated in total arc length to save on reflector material costs. In doing so, unfortunately, there will also be a small reduction in total concentration on the solar collector. Truncation at 10, 20, 30, and 40 percent of the arc length were taken into account and prepared for optical analysis. Figure 4.4 illustrates a 10% truncated, two-dimensional view of a reflector and absorber.

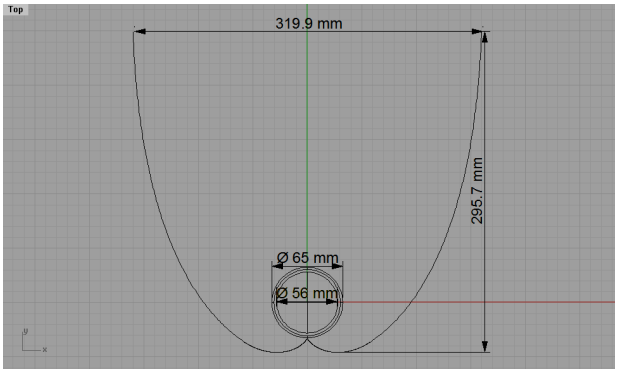

Figure 4.4. Two-dimensional view of XCPC reflector with absorber

Step 8: Three-dimensional modeling. After the various truncations were performed on the XCPC reflectors, each reflector variation was imported individually into a three dimensional nurbs modeling program. Each of the three conceptual designs, Jiang Tube, Dewar 47 and Dewar 58 was modeled for east-west and north-south orientations. In addition, each orientation had five truncation variations (0, 10, 20, 30 and 40 percent of the total arc length). In total, 30 XCPC reflectors were modeled and analyzed for optical efficiency. Each reflector half-curve was imported into Rhinoceros, then copied and

mirrored to complete the full reflector. A three-dimensional representation of the reflector and absorber can be seen in figure 4.5. Next, a computer replica of the solar collector was designed and inserted into each model variation. During this step, what is most important is the geometry of the objects. Each file was prepared for exporting into ray tracing software that will allow us to assign surface properties to the various components of the solar collector array.

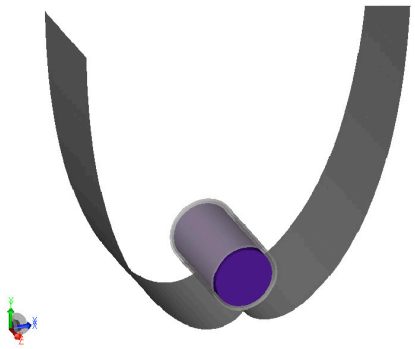

Figure 4.5. Three-dimensional model of full XCPC reflector with absorber

4.2 XCPC Design Specifications for Solar Thermal Absorbers

A summary of specifications for the design of each XCPC reflector for the various solar thermal collector units can be found in Tables 4.1 - 4.3. The acceptance angle for the horizontal orientation was prescribed as 34° and 60° for the vertical orientation. Each reflector design was then truncated at 10, 20, 30 and 40 percent to compare for reflector material used versus concentration ratio. Each solar thermal unit model will have 10 variations of the XCPC reflector with varying degrees of truncation and an east-west/north-south orientation.

Table 4.1. XCPC reflector design specifications for DEWAR 58

CONCEPT MODEL	ORIENTAITON	ACCEPT. ANGLE (°)	ABSORB. DIAM. (mm)	OUTER TUBE DIAM. (mm)	PERCENT TRUNC. (%)	ARC LENGTH (mm)	APERT. WIDTH (mm)
DEWAR 58	East-West	34	47	58	0	702.8	273.3
					10	630.6	271.7
					20	562.6	267.4
					30	498.2	260.3
					40	418.4	246.3
DEWAR 58	North-South	60	47	58	0	346.4	176.5
					10	313.4	175.3
					20	278.8	171.5
					30	242.8	164.5
					40	207.8	154.2

Table 4.2. XCPC reflector design specifications for DEWAR 47

CONCEPT MODEL	ORIENTAITON	ACCEPT. ANGLE (°)	ABSORB. DIAM. (mm)	OUTER TUBE DIAM. (mm)	PERCENT TRUNC. (%)	ARC LENGTH (mm)	APERT. WIDTH (mm)
DEWAR 47	East-West	34	37	47	0	562	216.9
					10	504.8	215.8
					20	450.8	212.6
					30	391.8	206.1
					40	336.8	196.5
DEWAR 47	North-South	60	37	47	0	275.6	140
					10	247.2	139
					20	220	136
					30	193.8	130.9
					40	166.2	122.9

Table 4.3. XCPC reflector design specifications for JIANG TUBE

CONCEPT MODEL	ORIENTAITON	ACCEPT. ANGLE (°)	ABSORB. DIAM. (mm)	OUTER TUBE DIAM. (mm)	PERCENT TRUNC. (%)	ARC LENGTH (mm)	APERT. WIDTH (mm)
JIANG TUBE	East-West	34	56	65	0	855.8	321.1
					10	768.2	320.3
					20	685.6	316.2
					30	595.2	307
					40	511	293.2
JIANG TUBE	North-South	60	56	65	0	408.4	207.4
					10	369	206
					20	327.8	201.5
					30	284.8	193
					40	246.2	181.5

5 Assessment of Optical Performance

Before a complete ray trace was performed on each solar collector array design, a simple calculation was performed to estimate the expected system optical efficiency. For each of the XCPC reflector variations, rays will cross through the glass cover glazing (two surfaces), be transformed by the reflector an average of one time, pass through the outer glass tube (two surfaces) and finish in the selective coated absorber. On each normal incidence passage through a glass/air boundary surface with n = 1.5, a fraction of 4.0% is reflected. Also, we know that the reflector mirror has around 95% efficiency and the absorber with selective coating has about 90% efficiency. The total system optical efficiency can be roughly estimated as n = 96% x 96% x 95% x 96% x 96% x 90% = 73%. As we can see from this calculation, theoretically it is possible to achieve a total system efficiency of at least 60% optical efficiency. However, we need to remember that these estimates are for an idealized concentrator and do not take into account the modifications that were made in the computer model design. We expect to see a decrease in overall system optical efficiency once a ray trace is performed.

In order to assess the optical efficiency of each of the solar collector array variations, a ray trace was performed using an optical performance modeling software. The number of rays used to determine the performance for each reflector was 100,000. Optical properties were assigned to materials and surfaces in the model. Once a light source is created in the software, rays propagate through the model with portions of the flux of each ray allocated for absorption, specular reflection and transmission, fluorescence and

scatter. Figure 5.1 shows an illustration of a solar thermal unit ray trace at normal incidence.

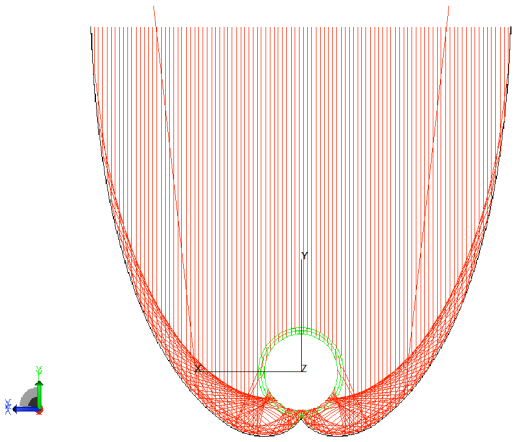

Figure 5.1. Ray Trace of Solar Thermal Collector Unit at Normal Incidence

5.1 Assessment of Optical Performance, Results for DEWAR 58

Results for the average optical efficiency and normal incidence efficiency of DEWAR 58 are shown in Tables/Charts 5.1 – 5.5. Results show average optical efficiencies for each of the Dewar 58 variations in the high 60's, ranging from 66.1%-67.2%. Optical efficiency at normal incidence was also in the 60's, ranging from 60.1%-64.3%. The similarities in optical efficiency between the different Dewar 58 variations is due to each model having an XCPC reflector that was specifically designed to maximize efficiency for its respective model solar collector specifications.

Truncation on the reflectors was performed in order to compare the tradeoff between concentration ratio and optical efficiency. The higher the truncation on a reflector, the greater the loss becomes in concentration ratio. For example, in DEWAR 58, east-west orientation, 0% truncation, we see a concentration ratio of 1.85, where as in the same

variation but with 40% truncation, we see a drop in concentration ratio of 1.67. After the data was analyzed, a level of 20% truncation was determined to be the best balance between optical efficiency and concentration ratio.

Following is efficiency data for Dewar 58 at 20% truncation in both east-west and north-south facing orientations. It is important to remember that the east-west orientation reflectors were designed to have a maximum acceptance angle of ±34° and the north-south orientation reflectors a maximum of ±60°. For the east-west orientation model at 20% truncation, we see the highest efficiency (71.44%) is achieved at 25°. For the north-south orientation model at 20% truncation, we see that the highest efficiency (72.92%) is achieved at 45°.

Table 5.1. Optical Performance Assessment Data for All Dewar 58 Variations

CONCEPT MODEL	ORIENTAITON	PERCENT TRUNC. (%)	CONCENT. RATIO	AVERAGE OPTICAL EFFIC (%)	NORMAL INCIDENCE EFFIC (%)
DEWAR 58	East-West	0	1.85	66.1	60.1
		10	1.84	66.5	60.3
		20	1.81	66.5	62.6
		30	1.76	67	63
		40	1.67	66.9	64.3
DEWAR 58	North-South	0	1.2	66.4	63
		10	1.19	67	62.8
		20	1.16	67.2	62.9
		30	1.11	66.8	62.4
		40	1.04	66.9	63.2

Chart 5.2. Optical Efficiency by Incidence Angle for Dewar 58, 20% Truncation, East-West Orientation

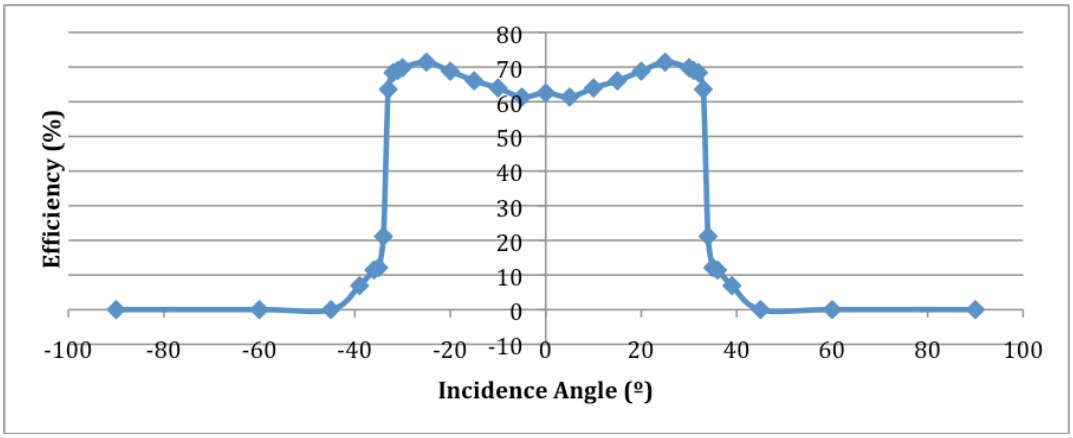

Table 5.3. Optical Performance Assessment Data by Incidence Angle for Dewar 58, 20% Truncation, East-West Orientation

Incidence Angle (º)	Optical Efficiency (%)	Incidence Angle (º)	Optical Efficiency (%)
0	62.55	-90	0
5	61.34	-60	0
10	63.97	-45	0
15	66.04	-39	6.92
20	68.81	-36	11.43
25	71.42	-35	12.11
30	69.81	-34	21.15
31	69.03	-33	63.57
32	68.39	-32	68.39
33	63.57	-31	69.03
34	21.15	-30	69.81
35	12.11	-25	71.42
36	11.43	-20	68.81
39	6.92	-15	66.04
45	0	-10	63.97
60	0	-5	61.34
90	0	0	62.55

Chart 5.4. Optical Performance Assessment by Incidence Angle for Dewar 58, 20% Truncation, North-South Orientation

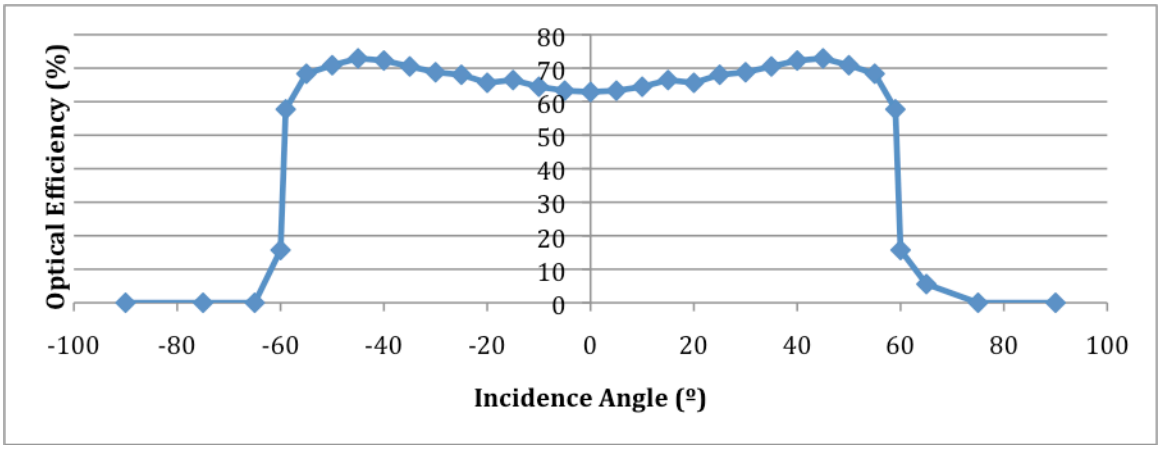

Table 5.5. Optical Performance Assessment Data by Incidence Angle for Dewar 58, 20% Truncation, North-South Orientation

Incidence Angle (º)	Optical Efficiency (%)	Incidence Angle (º)	Optical Efficiency (%)
0	62.91	-90	0
5	63.29	-75	0
10	64.46	-65	0
15	66.46	-60	15.725
20	65.64	-59	57.72
25	68.035	-55	68.335
30	68.78	-50	70.875
35	70.505	-45	72.92
40	72.28	-40	72.28
45	72.92	-35	70.505
50	70.875	-30	68.78
55	68.335	-25	68.035
59	57.72	-20	65.64
60	15.725	-15	66.46
65	5.57	-10	64.46
75	0	-5	63.29
90	0	0	62.91

5.2 Assessment of Optical Performance, Results of DEWAR 47

The average optical efficiency and normal incidence efficiency for Dewar 47 is shown in Tables/Charts 5.6 – 5.10. Results show average optical efficiencies for each of the Dewar 47 variations in the high 60's, ranging from 65.3%-67.8%. Optical efficiency at normal incidence was in the high 50's and low 60's, ranging from 58.5%-63.1%.

As in Dewar 58, truncation on the reflectors was performed. The higher the truncation on a reflector, the greater the loss becomes in concentration ratio. In DEWAR 47, east-west orientation, 0% truncation, we see a concentration ratio of 1.87, where as in the same variation but with 40% truncation, we see a drop in concentration ratio of 1.69. After the data was analyzed, a level of 20% truncation was determined to be the best balance between optical efficiency and concentration ratio with material cost.

Following is efficiency data for Dewar 47 at 20% truncation in both east-west and north-south facing orientations. For the east-west orientation model at 20% truncation, we see the highest efficiency (71.03%) is achieved at 25°. For the north-south orientation model at 20% truncation, we see that the highest efficiency (72.85%) is achieved at 40°.

Table 5.6. Optical Performance Assessment Data for All Dewar 47 Variations

CONCEPT MODEL	ORIENTAITON	PERCENT TRUNC. (%)	CONCENT. RATIO	AVERAGE OPTICAL EFFIC (%)	NORMAL INCIDENCE EFFIC (%)
DEWAR 47	East-West	0	1.87	65.3	58.5
		10	1.86	65.8	60.1
		20	1.83	66.2	61.8
		30	1.77	65.9	61.6
		40	1.69	66.2	63.1
DEWAR 47	North-South	0	1.2	66.1	62.7
		10	1.2	66.3	60.2
		20	1.17	67.1	62.4
		30	1.13	67.6	61.6
		40	1.06	67.8	62.3

Chart 5.7. Optical Performance Assessment by Incidence Angle for Dewar 47, 20% Truncation, East-West Orientation

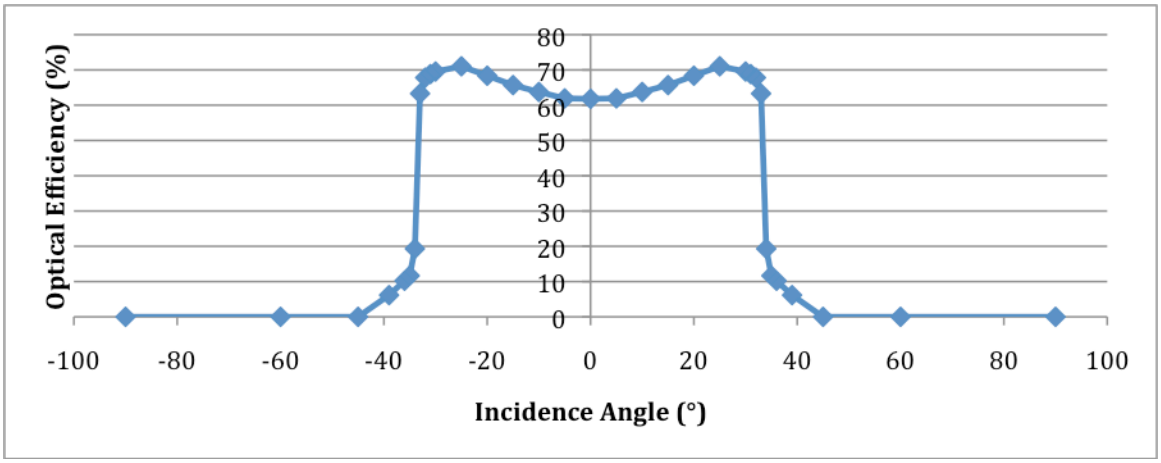

Table 5.8. Optical Performance Assessment Data by Incidence Angle for Dewar 47, 20% Truncation, East-West Orientation

Incidence Angle (º)	Optical Efficiency (%)	Incidence Angle (º)	Optical Efficiency (%)
0	61.8	-90	0
5	61.93	-60	0
10	63.75	-45	0
15	65.70	-39	6.16
20	68.36	-36	10.23
25	71.03	-35	11.66
30	69.54	-34	19.31
31	68.82	-33	63.3
32	67.81	-32	67.81
33	63.3	-31	68.82
34	19.31	-30	69.54
35	11.66	-25	71.03
36	10.23	-20	68.36
39	6.16	-15	65.70
45	0	-10	63.75
60	0	-5	61.93
90	0	0	61.8

Chart 5.9. Optical Performance Assessment by Incidence Angle for Dewar 47, 20% Truncation, North-South Orientation

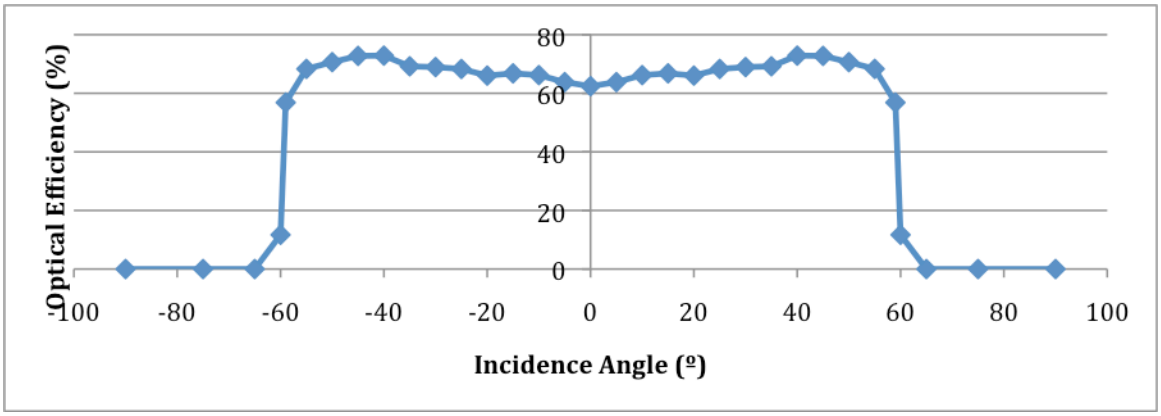

Table 5.10. Optical Performance Assessment Data by Incidence Angle for Dewar 47, 20% Truncation, North-South Orientation

Incidence Angle (º)	Optical Efficiency (%)	Incidence Angle (º)	Optical Efficiency (%)
0	62.42	-90	0
5	63.8	-75	0
10	66.2	-65	0
15	66.80	-60	11.69
20	66.03	-59	56.84
25	68.3	-55	68.32
30	68.94	-50	70.63
35	69.2	-45	72.76
40	72.85	-40	72.85
45	72.76	-35	69.2
50	70.63	-30	68.94
55	68.32	-25	68.3
59	56.84	-20	66.03
60	11.69	-15	66.80
65	0	-10	66.2
75	0	-5	63.8
90	0	0	62.42

5.3 Assessment of Optical Performance, Results of JIANG TUBE

The average optical efficiency and normal incidence efficiency for Jiang Tube is shown in Tables/Charts 5.11 – 5.15. Results show average optical efficiencies for each of the JIANG TUBE variations in the high 60's, ranging from 67.3%-68.4%. Optical efficiency at normal incidence was in the low 60's, ranging from 62.8%-64.9%.

As in the previous two XCPC reflector models, truncation on the reflectors was performed in order to compare the tradeoff between concentration ratio and optical efficiency. In the JIANG TUBE, east-west orientation, 0% truncation, we see a concentration ratio of 1.83, where as in the same variation but with 40% truncation, we

see a drop in concentration ratio of 1.67. After the data was analyzed, a level of 20% truncation was determined to be the best balance between optical efficiency and concentration ratio with material cost.

Following is efficiency data for JIANG TUBE at 20% truncation in both east-west and north-south facing orientations. It is important to remember that the east-west orientation reflectors were designed to have a maximum acceptance angle of ±30° and the north-south orientation reflectors a maximum of ±60°. For the east-west orientation model at 20% truncation, we see the highest efficiency (71.53%) is achieved at 25°. For the north-south orientation model at 20% truncation, we see that the highest efficiency (72.46%) is achieved at 40% truncation.

Table 5.11. Optical Performance Assessment Data for All JIANG TUBE Variations

CONCEPT MODEL	ORIENTAITON	PERCENT TRUNC. (%)	CONCENT. RATIO	AVERAGE OPTICAL EFFIC (%)	NORMAL INCIDENCE EFFIC (%)
JIANG TUBE	East-West	0	1.83	67.5	62.8
		10	1.82	67.6	63.2
		20	1.8	67.5	63.9
		30	1.75	67.5	64.3
		40	1.67	67.8	64.7
JIANG TUBE	North-South	0	1.18	67.3	63.8
		10	1.17	68.2	64.6
		20	1.15	68.4	64.8
		30	1.1	68.3	64.9
		40	1.03	68.2	63.9

Chart 5.12. Optical Performance Assessment by Incidence Angle for JIANG TUBE, 20% Truncation, East-West Orientation

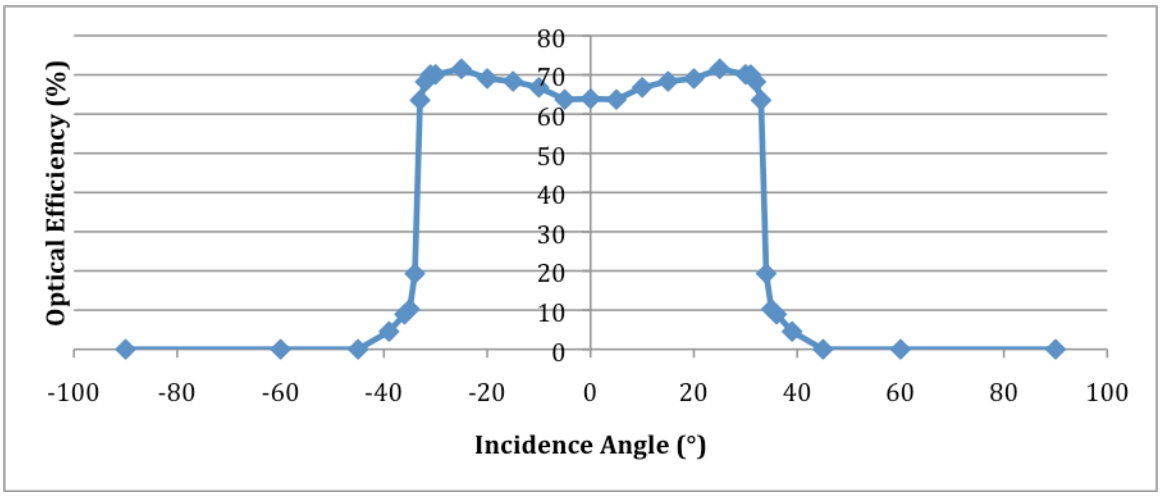

Table 5.13. Optical Efficiency Data by Incidence Angle for JIANG TUBE, 20% Truncation, East-West Orientation

Incidence Angle (º)	Optical Efficiency (%)	Incidence Angle (º)	Optical Efficiency (%)
0	63.9	-90	0
5	63.71	-60	0
10	66.8	-45	0
15	68.33	-39	4.54
20	69.05	-36	8.95
25	71.53	-35	10.24
30	70.1	-34	19.32
31	70.04	-33	63.54
32	68.23	-32	68.23
33	63.54	-31	70.04
34	19.32	-30	70.1
35	10.24	-25	71.53
36	8.95	-20	69.05
39	4.54	-15	68.33
45	0	-10	66.8
60	0	-5	63.71
90	0	0	63.9

Chart 5.14. Optical Efficiency by Incidence Angle for JIANG TUBE, 20% Truncation, North-South Orientation

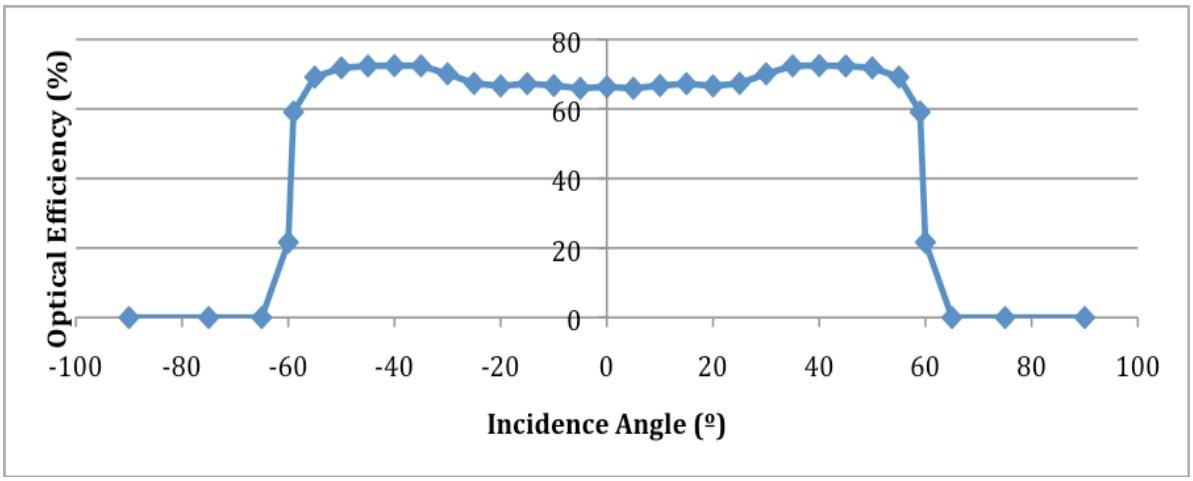

Table 5.15. Optical Efficiency Data by Incidence Angle for JIANG TUBE, 20% Truncation, North-South Orientation

Incidence Angle (º)	Optical Efficiency (%)	Incidence Angle (º)	Optical Efficiency (%)
0	66.38	-90	0
5	65.93	-75	0
10	66.74	-65	0
15	67.27	-60	21.65
20	66.62	-59	59.12
25	67.34	-55	69.17
30	70.11	-50	71.81
35	72.4	-45	72.36
40	72.46	-40	72.46
45	72.36	-35	72.4
50	71.81	-30	70.11
55	69.17	-25	67.34
59	59.12	-20	66.62
60	21.65	-15	67.27
65	0	-10	66.74
75	0	-5	65.93
90	0	0	66.38

6 Conclusion

The objective of this thesis was to provide a preliminary performance assessment of optical components for each of the three high temperature solar thermal collector concept designs. As shown through this paper, for each of the three design concepts, DEWAR 58, DEWAR 47 and JIANG Tube, achieving optical efficiencies above 60% is possible. Table 6.1 summarizes the optical performance for each reflector variation in the horizontal (east-west) orientation.

Table 6.1. Summary of XCPC reflector optical assessment, horizontal orientation

Reflector Design (Type)	Orientation	Reflector Truncation (%)	Optical Efficiency (>60%)	Concentration Ratio (>1.5x)	Ideal Reflector Design
DEWAR 58	East-West	0	√	√	√
		10	√	√	√
		20	√	√	√
		30	√	√	√
		40	√	√	√
DEWAR 47	East-West	0	√	√	√
		10	√	√	√
		20	√	√	√
		30	√	√	√
		40	√	√	√
JIANG TUBE	East-West	0	√	√	√
		10	√	√	√
		20	√	√	√
		30	√	√	√
		40	√	√	√

The concentration ratio of reflectors with horizontal orientation was above 1.5x; however, the concentration for the vertically orientated reflectors did not surpass 1.5. This is due to the tradeoffs in concentration vs. efficiency. Although, the vertically

oriented models had lower concentration ratios, they performed as well in overall optical performance due to better optical efficiencies than the horizontally oriented reflectors. In summary any of these variations of reflectors will optically perform at a level satisfactory such that the solar collector unit can achieve temperatures above 200ºC. Table 6.2 summarizes the optical performance for each reflector variation in the vertical (north-south) orientation. A complete detailed optical performance summary for both directional orientations can be found in Table 6.3.

Table 6.2. Summary of XCPC reflector optical assessment, vertical orientation

Reflector Design (Type)	Orientation	Reflector Truncation (%)	Optical Efficiency (>60%)	Concentration Ratio (>1.5x)	Ideal Reflector Design
DEWAR 58	North-South	0	√	X	√
		10	√	X	√
		20	√	X	√
		30	√	X	√
		40	√	X	√
DEWAR 47	North-South	0	√	X	√
		10	√	X	√
		20	√	X	√
		30	√	X	√
		40	√	X	√
JIANG TUBE	North-South	0	√	X	√
		10	√	X	√
		20	√	X	√
		30	√	X	√
		40	√	X	√

Table 6.3. Complete summary of XCPC reflector performance assessment

High Temperature Solar Thermal Collector
Concept Model Optical Analysis Summary

CONCEPT MODEL	ORIENTATION	ACCEPT. ANGLE (°)	ABSORB. DIAM. (mm)	OUT. TUBE DIAMETER (mm)	PERCENT TRUNC. (%)	ARC LENGTH (mm)	APERT. WIDTH (mm)	CONCENT. RATIO	AVERAGE OPTICAL EFFIC. (%)	NORMAL INCIDENCE EFFIC. (%)
JIANG TUBE	East-West	34	56	65	0	855.8	321.1	1.83	67.5	62.8
					10	768.2	320.3	1.82	67.6	63.2
					20	685.6	316.2	1.8	67.5	63.9
					30	595.2	307	1.75	67.5	64.3
					40	511	293.2	1.67	67.8	64.7
DEWAR 58	East-West	34	47	58	0	702.8	273.3	1.85	66.1	60.1
					10	630.6	271.7	1.84	66.5	60.3
					20	562.6	267.4	1.81	66.5	62.6
					30	498.2	260.3	1.76	67	63
					40	418.4	246.3	1.67	66.9	64.3
DEWAR 47	East-West	34	37	47	0	562	216.9	1.87	65.3	58.5
					10	504.8	215.8	1.86	65.8	60.1
					20	450.8	212.6	1.83	66.2	61.8
					30	391.8	206.1	1.77	65.9	61.6
					40	336.8	196.5	1.69	66.2	63.1
JIANG TUBE	North-South	60	56	65	0	408.4	207.4	1.18	67.3	63.8
					10	369	206	1.17	68.2	64.6
					20	327.8	201.5	1.15	68.4	64.8
					30	284.8	193	1.1	68.3	64.9
					40	246.2	181.5	1.03	68.2	63.9
DEWAR 58	North-South	60	47	58	0	346.4	176.5	1.2	66.4	63
					10	313.4	175.3	1.19	67	62.8
					20	278.8	171.5	1.16	67.2	62.9
					30	242.8	164.5	1.11	66.8	62.4
					40	207.8	154.2	1.04	66.9	63.2
DEWAR 47	North-South	60	37	47	0	275.6	140	1.2	66.1	62.7
					10	247.2	139	1.2	66.3	60.2
					20	220	136	1.17	67.1	62.4
					30	193.8	130.9	1.13	67.6	61.6
					40	166.2	122.9	1.06	67.8	62.3

One of the tasks outside of this thesis is to build a prototype collector unit in order to research optical performance, total unit efficiency performance testing and system optimization. After improving the reflector technology and incorporating a new evacuated thermal absorber design, researchers at UC MERI later constructed and tested. After further improvements and adjustments, a 10kW prototype was manufactured and tested at the NASA/Ames facility. This manufacturable prototype has been in operation since spring of 2008.

Measurements of the manufactured prototype, produced by UC MERI, show results similar to those predicted with the conceptual models in this paper. Chart 6.4 shows the real-life optical performance results of the East-West orientation. Results show an angular acceptance of 90% for the collector in the range of ±32.5 degrees. In practical terms, it means that the prototype is performing at or above expectations. Chart 6.5 shows an average optical efficiency of 66.4% for the prototype reflector in the North-South orientation. These figures reflect the predicted performance described in this thesis.

Chart 6.4. Angular Acceptance for Manufactured Prototype, North-South Orientation

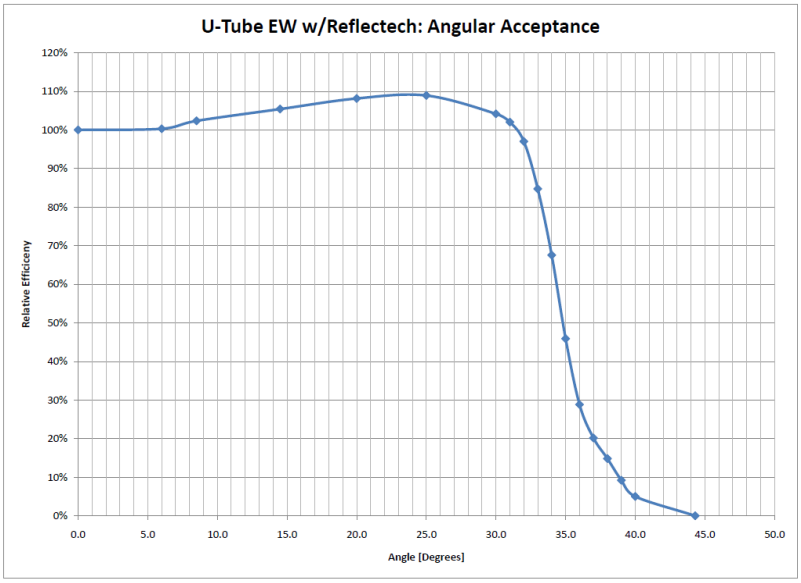

Chart 6.5. Optical Efficiency by Incidence Angle for Manufactured Prototype, North-South Orientation

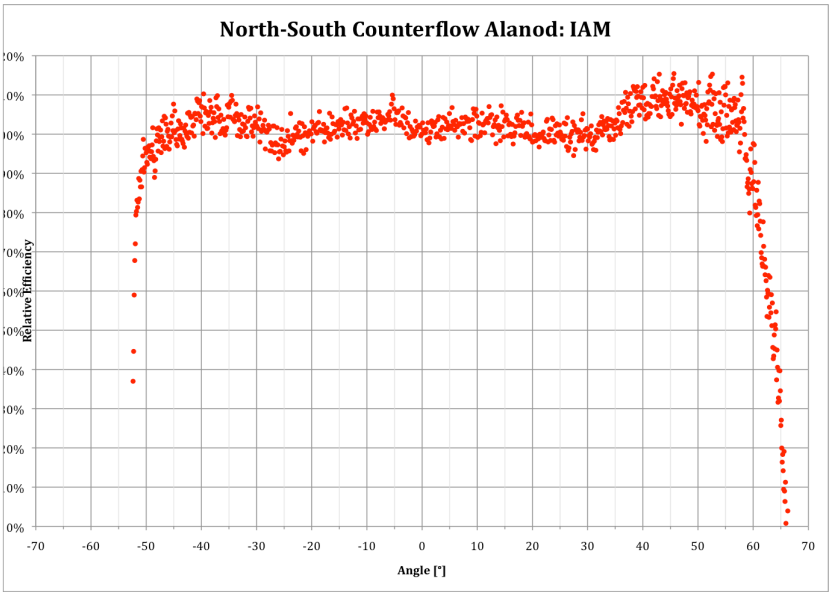

As demonstrated through this paper, the solar thermal collector can replace natural gas used for heat and space cooling with solar energy, leading to a more cost effective use of natural resources and decreased air emissions. Given that conventional flat plate collectors, and even the Winston-Series CPC manufactured by Solargenix Energy, cannot operate with a positive efficiency at temperatures above 250°F, this project has stimulated a major advance in practical solar heating, cooling and power generation. So much so, that a new company was recently created as a spinout of SolFocus to commercialize the XCPC technology. This new company is called B2U Solar, and it is based in Mountain View, CA. B2U Solar is already focusing its commercial efforts on immediate high potential areas, including: HVAC employing double-effect absorption cooling; industrial/commercial boiler or oil heater augmentation; and process heat.

Researchers at UC Merced are also working with industry on other high impact areas for this technology. Evaluations are under way that could lead a new research program focused on harnessing solar thermal energy for water desalination projects in the California Central Valley and beyond.

REFERENCES

Cengel, Y.A. (2006, 3rd ed.) Heat and Mass Transfer: A Practical Approach. Boston: McGraw-Hill

Chaves, J. (2008, 1st ed.) Introduction to nonimaging optics. Boca Raton: CRC Press.

Der Minassians, A., K. H. Aschenbach, et al. (2003). *Low-Cost Distributed Solar-Thermal-Electric Power Generation*. Nonimaging optics: Maximum efficiency light transfer VII: San Diego, CA (USA). SPIE.

González, M. I. and L. R. Rodríguez (2007). "Solar powered adsorption refrigerator with CPC collection system: Collector design and experimental test". Energy Conversion and Management **48**(9): 2587-2594.

Goswami, Y. et al (2000). Principles of Solar Engineering. Phililidelphia: Taylor & Francis.

Hinterberger, H., and Winston, R. (1966a). Efficient light coupler for threshold Cerenkov counters. Rev. Science Instruments.

Kalogirou, S. A. (2004). "Solar thermal collectors and applications". Progress in Energy and Combustion Science **30**(3): 231-295.

Philibert, C. (2005). The present and future of solar thermal energy as a primary source of energy. International Energy Agency. Paris (France).

Rabl, A. (1976). "Comparison of Solar Concentrators". Solar Energy **18**(2): 93-111.

Rabl, A. (1976). "Solar concentrators with maximal concentration for cylindrical absorbers". Applied Optics **15**(7): 1871-1873.

Rabl, A., N. B. Goodman, et al. (1979). "Practical design considerations for CPC solar collectors". Solar Energy **22**(4): 373-381.

Rabl, A. and R. Winston (1976). "Ideal concentrators for finite sources and restricted angles". Applied Optics **16**(11): 2880-2883.

Ries, H., and Rabl (1994). Edge ray principle of nonimaging optics. Journal of Optical Science Am. A 11, 2627-2632.

Welford, W.T., Winston, R (1989). High Collection Nonimaging Optics. Chicago: Academic Press

Winston, R. (1970). Light Collection within the framework of geometrical optics. Journal of Optical Science Am. A 60, 245-247.

Winston, R. (1974). Principles of Solar Concentrators of a novel design. Solar Energy 16, 89-95.

Winston, R., and Hinterberger, H. (1975). Principles of cylindrical concentrators for solar energy. Solar Energy 17, 255-258

Winston, R., Minano, J., et al. (2005). Nonimaging Optics. San Diego, CA: Elsevier Inc.